Published OnlineFirst June 9, 2009; DOI: 10.1158/1535-7163.MCT-08-1012



# The antiproliferative cytostatic effects of a self-activating viridin prodrug

**Adam Smith,[1] Joseph Blois,[1] Hushan Yuan,[1] Elena Aikawa,[1] Christian Ellson,[3] Jose-Luiz Figueiredo,[1] Ralph Weissleder,[2] Rainer Kohler,[1] Michael B. Yaffe,[3] Lewis C. Cantley,[2] and Lee Josephson[1]**

**[1]Center for Molecular Imaging Research, Massachusetts General Hospital and Harvard Medical School, Charlestown, Massachusetts; [2]Department of Systems Biology, Harvard Medical School and Division of Signal Transduction, Beth Israel Deaconess Medical Center, Louis Pasteur, Boston, Massachusetts; and [3]Koch Institute for Integrative Cancer Research, Department of Biology, Cambridge, Massachusetts**

## Abstract

**Although viridins like wortmannin (Wm) have long been examined as anticancer agents, their ability to self-activate has only recently been recognized. Here, we describe the cytostatic effects of a self-activating viridin (SAV), which is an inactive, polymeric prodrug. SAV self-activates to generate a bioactive, fluorescent viridin NBD-Wm with a half-time of 9.2 hours. With cultured A549 cells, 10 μmol/L SAV caused growth arrest without inducing apoptosis or cell death, a cytostatic action markedly different from other chemotherapeutic agents (vinblastine, camptothecin, and paclitaxel). *In vivo*, a SAV dosing of 1 mg/kg once in 48 hours (i.p.) resulted in growth arrest of an A549 tumor xenograft, with growth resuming when dosing ceased. With a peak serum concentration of SAV of 2.36 μmol/L (at 2 hours post i.p. injection), the concentration of bioactive NBD-Wm was 41 nmol/L based on the partial inhibition of neutrophil respiratory burst. Therefore, SAV was present as an inactive prodrug in serum (peak = 2.36 μmol/L), which generated low concentrations of active viridin (41 nmol/L). SAV is a prodrug, the slow release and cytostatic activities of which suggest that it might be useful as a component of metronomic-based chemotherapeutic strategies. [Mol Cancer Ther 2009;8(6):1666–75]**

Received 11/11/08; revised 3/24/09; accepted 4/10/09; published OnlineFirst 6/9/09.

**Grant support:** NIH grants T32P50-CA86355, RO1-EB004472, R01-GM059281, and T32-CA079443. C. Ellson was funded by the Charles A. King Trust, Bank of America, Co-Trustee.

The costs of publication of this article were defrayed in part by the payment of page charges. This article must therefore be hereby marked *advertisement* in accordance with 18 U.S.C. Section 1734 solely to indicate this fact.

**Requests for reprints:** Lee Josephson, Massachusetts General Hospital, Center for Molecular Imaging Research, 149 13th Street, Charlestown, MA 02129. Phone: 617-726-6478; Fax: 617-726-5708. E-mail: ljosephson@mgh.harvard.edu



doi:10.1158/1535-7163.MCT-08-1012

## Introduction

Many protocols use high doses of chemotherapeutic agents to maximize tumor cell killing, followed by a recovery period and then by additional high-dose treatments. Low molecular weight, high-affinity, selective kinase inhibitors have often been developed using a similar rationale, seeking to inhibit the kinases that drive the proliferation (or survival) of cancer cells in a select subset of cancer patients, with the goal of eradicating the tumor. An alternative, metronomic chemotherapeutic approach uses low doses of agents with the goal of inhibiting tumor growth (1). Here, we describe a polymeric, slow-viridin-releasing prodrug that has cytostatic properties that may make it useful as a metronomic chemotherapeutic agent.

The viridins are fungally derived, steroid-like structures with a furan ring, the most studied of which is wortmannin (Wm; refs. 2, 3). Unlike steroids, viridins are chemically reactive compounds, irreversibly modifying target kinases (4) and reacting with amino acids under physiologic conditions (5). Although viridins have been examined for well over a decade as anticancer agents (6–8), their ability to self-activate after modification has only recently been recognized (5, 9, 10). Our self-activating viridin (SAV) prodrug exploits that feature of viridin chemistry, namely a slow self-activation to generate low concentrations of the active viridin (Wm) in biological fluids. Because many carrier-based and targeted compounds use some feature of the intracellular environment (e.g., enzymes, low intracellular pH, disulfide reduction) to cleave a bond between a carrier and an active agent, and SAV generates Wm in PBS, we term it a "self-activating viridin" based on this unique feature (5, 9, 10). Unlike most other kinase inhibitors, SAV is inactive in the form synthesized, but then slowly self-activates to generate the active viridin, NBD-Wm, as shown in Fig. 1A. For a comprehensive review of carrier-based prodrugs and their release mechanisms, see ref. (11). As a control for SAV in some experiments, we developed in parallel a nonactivating version of Wm with the same physical properties of SAV. This compound is termed "nonactivating viridin" (NAV; ref. 9).

The current study builds on and extends our earlier work with SAV (5, 9, 10) in several directions. First, we attached a Cy5 fluorochrome to the carrier dextran so that the pharmacokinetics of SAV and serum concentration could be determined. Second, we have shown that the antiproliferative activity of SAV in animals requires viridin release, by demonstrating the inactivity of NAV in this regard. Third, we have shown the antiproliferative effects of SAV differ from the cytotoxic responses produced by other chemotherapeutic agents. Finally, we examined the intratumoral distribution of SAV in a xenograft tumor model and have shown the association of viridin with peripheral, highly vascularized sections of the tumor. The low concentrations of active

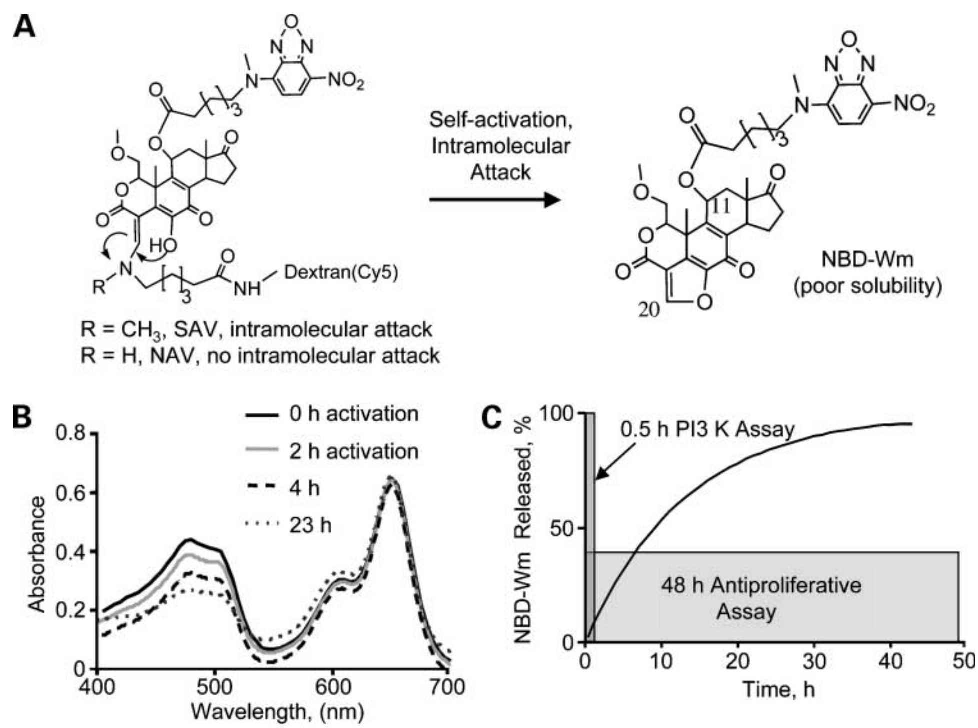


**Figure 1.** Structure of SAV and released viridin, NBD-Wm. **A,** structures of SAV, NBD-Wm, and a control NAV. Positions of C20 and C11 are modified on NBD-Wm. When R is $CH_3$, that is, with SAV, self-activation through an intramolecular attack generates the active viridin (NBD-Wm). When released from the hydrophilic dextran carrier of SAV, NBD-Wm has low water solubility and precipitates. **B,** absorption spectra from supernatants of SAV as a function of incubation time. Released NBD-Wm is removed by its poor solubility. Absorbance from NBD at 480 nm decreased whereas absorbance at 650 nm due to Cy5 was constant due to the solubility of SAV or dextran(Cy5). A half-time of release of 9.2 h was calculated for NBD-Wm release from the decrease in 480-nm absorption. **C,** generation of NBD-Wm by SAV relative to the duration of assays. SAV self-activation (*black curve*) was partial during the 0.5-h kinase assay but nearly complete during the 48-h antiproliferative assay.

viridin generated by SAV in blood make it an attractive agent for use in metronomic chemotherapeutic strategies, where a goal is to maintain low but effective levels of agents that exert either antitumor cell effects or antiangiogenic effects (1).

## Materials and Methods

### Syntheses

Structures of the compounds used are shown in Fig. 1A. NBD-Wm was synthesized as described (12). The syntheses of SAV and NAV using NBD-Wm or Wm have been described (9, 10). An NHS ester of Cy5 (GE Amersham Biosciences) was attached to a 70 kDa amino dextran carrier (InVitrogen), to obtain a molar ratio of Cy5/dextran (0.58) determined spectrophotometrically. For SAV, there was an average of 3.7 moles of NBD-Wm attached per mole of dextran, determined from the absorbance of NBD at 490 nm using an NBD standard. NAV was prepared by substituting amino hexanoic acid for *N*-methyl hexanoic acid as the linker. NAV had an average of NBD-Wm to dextran ratio of 2.8. SAV or NAV are expressed as moles or weights of NBD-Wm. In Fig. 4A and B, the NBD and Cy5 fluorochromes were omitted in SAV design as a cost-saving measure. Because NBD-Wm and Wm have similar activities, before and after attachment to dextran, we refer to them as viridins (9, 12).

### Assay for Self-activation

A solution of SAV or NAV (1.5 mmol/L Wm equivalents) in 300 μL in PBS (pH 6.8) was incubated at 37°C. Released NBD-Wm was removed by centrifugation (5 min, 13,000 rpm) in a microfuge. Wm formation was obtained from a loss of absorbance at 480 nm. Data fit a first-order decay process with coefficients of correlation of >0.90 in all cases.

### Bioactivity of Compounds

The antiproliferative assay used A549 cells (12). To obtain the uptake of compounds, A549 cells were incubated with 10 μmol/L of Wm as NBD-Wm, SAV, or NAV for the indicated time. Cells were detached with trypsin and fluorescence was determined by fluorescence-activated cell sorting (FACS). Wm is growth inhibitory to cells in culture, with its effects on A549 cells typical of a wide range of cancer cell lines.

### NBD Immunohistochemistry for Intratumor Distribution

Tumors were excised, frozen in optimum cutting temperature compound (Sakura Finetek), and sectioned in 5-μm slices. Adjacent sections were then preincubated with 0.3% hydrogen peroxide to inhibit endogenous peroxidase activity and then incubated with primary polyclonal rabbit anti-4-fluoro-7-nitrobenzofurazan antibody (AbD Serotec). After washing with PBS, a secondary biotinylated anti-rabbit IgG (Vector Laboratories, Inc.) was applied followed by avidin-peroxidase complex (Vector Laboratories). The reaction was visualized with 3-amino-9-ethyl carbazole (Sigma Chemical Co). Sections were counterstained with Mayer's hematoxylin solution (Sigma) and mounted. Images were captured with a digital camera (Nikon DXM1200-F) using imaging software ACT-1 (version 2.63).

### A549 Xenograft

Two million cells in 0.1 mL PBS were implanted s.c. into the right flank of 5- to 8-wk-old nu/nu mice. Tumor growth was monitored by measurements with digital calipers, and tumor volume was calculated with the equation $V = 0.5 \times L \times W^2$. Once tumors reached ~100 $mm^3$, treatment commenced administering SAV or NAV (1 mg/kg, i.p.).

Published OnlineFirst June 9, 2009; DOI: 10.1158/1535-7163.MCT-08-1012



### Cell Cycle Analysis

Procedure was from ref. (13) with minor modifications. Cells (~$10^6$) were harvested by trypsinization and centrifuged at 200 × $g$ for 5 min. The resulting cell pellet was resuspended in 0.5 mL PBS and vortexed to achieve a single cell suspension. To fix cells, 5 mL of 70% ethanol were added and the cell suspension was incubated overnight on ice. After fixation, cells were pelleted by centrifugation at 200 × $g$ for 5 min. Cells were then resuspended in 5 mL PBS and again centrifuged at 200 × $g$ for 5 min. For staining, the cell pellet was resuspended in 1 mL propidium iodide/Triton X-100 (0.1% v/v Triton X-100 in PBS, 0.20 mg/mL propidium iodide) and incubated for 15 min at 37°C. Stained cells were then analyzed by flow cytometry (488-nm excitation, FL2 channel). Data analysis was done using the Watson cell cycle model and FlowJo analysis software. Statistical analyses were done using Prism 4.0 (GraphPad Software). ANOVA tests were applied with $P$ values of less than 0.05 considered significant. Uncertainties are SEs for at least three determinations.

### Assay for Apoptotic and Dead Cells

Cells were cultured in a 24-well plate with SAV or a chemotherapeutic agent for 48 h. Cells were detached by incubation with 200 µL of trypsin EDTA (InVitrogen) for 5 to 10 min at 37°C, combined with any spontaneously detached cells, washed and pelleted (200 × $g$ for 5 min). Cells were resuspended in 300 µL of Dulbecco's PBS, 1% FCS and stained with propidium iodide and APC-Annexin V (Molecular Probes), according to the manufacturer's protocol. Cells were then resuspended in Dulbecco's PBS and analyzed with a FACSCalibur flow cytometer in the FL3 (PI) and FL4 (APC) channels. Apoptotic cells were scored as FL4 single positive, dead cells were considered PI positive, and live cells were double negative. Quadrant statistics were analyzed using CellQuest software and gate placement was aided with the use of positive and negative controls.

### SAV Pharmacokinetics

The transfer of SAV from the blood to interstitium after i.v. injection, or from peritoneum to the blood and from the blood to the interstitium after i.p. injection was monitored as ear vessel fluorescence using intravital fluorescence microscopy. A multichannel confocal laser-scanning microscope (Radiance 2100, Bio-Rad) on a Nikon Eclipse E600 microscope (Nikon) with a 20× air objective was used. Nu/nu mice ($n$ = 3) were anesthetized (2.0% isoflurane) and injected (tail vein) with 100 µg of a 155-kDa tetramethylrhodamine-labeled dextran (Sigma-Aldrich), to visualize vessels before SAV was injected. SAV, 1 mg/kg, i.p., was injected and images of vessels were collected using the Lasersharp 2000 program (Bio-Rad). For each time point, three high-intensity regions of interest recognizable as vasculature were defined from Cy5 fluorescence using ImageJ

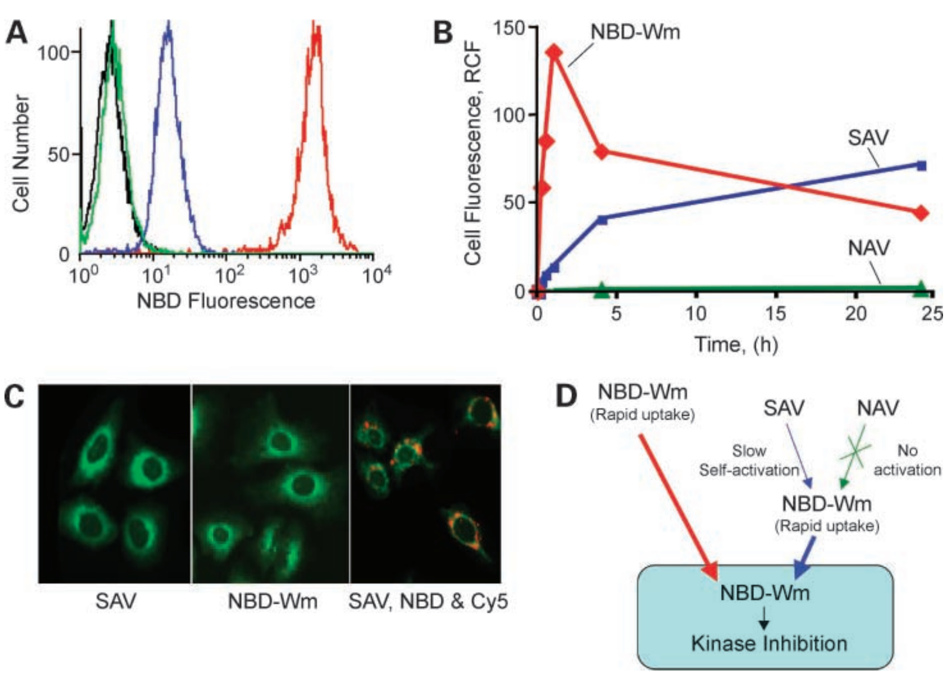


**Figure 2.** Behavior of SAV with cells *in vitro*. **A,** FACS analysis showing the uptake of compounds at 1 h. Cells were incubated with 10 µmol/L NBD-Wm as NBD-Wm (*red*), as SAV (*blue*), or as NAV (*green*). Control cells are shown in black. A RCF was calculated from the mean fluorescence intensity of treated divided by that of control cells. **B,** time dependence of internalization of NBD-Wm for cells treated with 10 µmol/L NBD-Wm as NBD-Wm, SAV, or NAV. Small-molecule NBD-Wm entered cells rapidly. NBD-Wm from SAV entered cells slowly and increased over 24 h, corresponding with the slow self-activation of SAV and the slow release of NBD-Wm. NBD-Wm supplied as NAV, which was not released, did not enter cells. **C,** fluorescence micrographs of cells incubated with SAV or NBD-Wm. NBD fluorescence is green and Cy5 fluorescence is red. Incubation times were 1 h for NBD-Wm and SAV (*left* and *center*), and 24 h for SAV, NBD, and Cy5 (*right*). The brightness of images was adjusted to be similar for comparison of intracellular localization. **D,** a model of NBD-Wm uptake when cells were incubated with SAV. The colors of the arrows correspond to colors from **A** and **B**. Thickness of arrows indicates relative rate. SAV self-activated to release NBD-Wm into media, followed by its rapid uptake into cells.

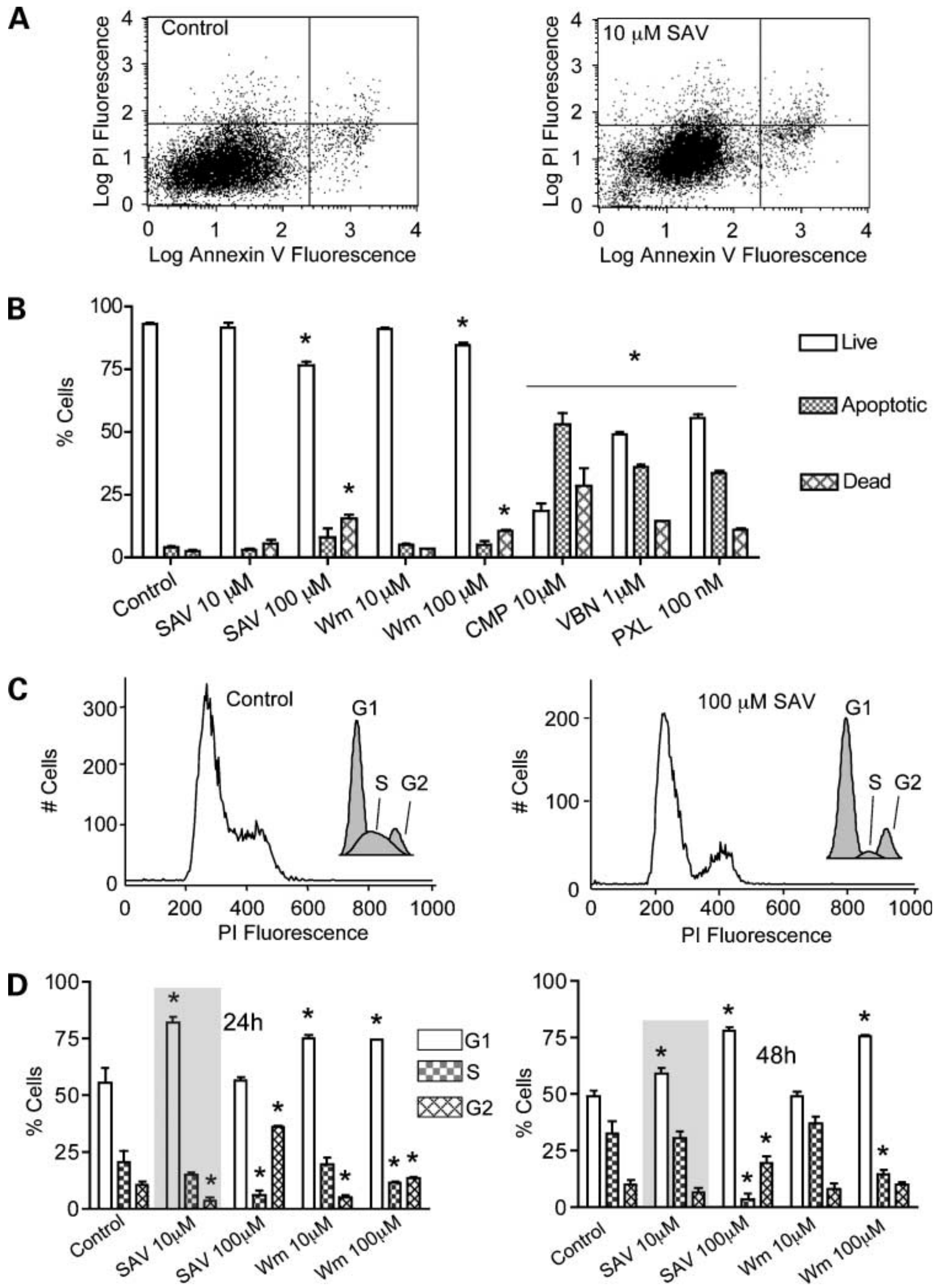


**Figure 3.** Antiproliferative and cytostatic effect of SAV on cultured A549 cells. **A,** dual-wavelength FACS of propidium iodide (*PI*) uptake (*Y* axis) and APC-Annexin V binding (*X* axis). Control cells (*left*) or cells treated with 10 µmol/L SAV for 48 h (*right*). **B,** data from **A**, as well as additional points are provided. *Asterisks,* statistical significance at $P < 0.05$. *Error bars,* SE of three determinations. Treatment of cells with an antiproliferative concentration of 10 µmol/L SAV, 10 times higher than the antiproliferative $IC_{50}$ of 1.05 µmol/L, was without a cytotoxic effect, defined as a failure to increase the proportions of dead or apoptotic cells. Other chemotherapeutic agents [camptothecin (*CMP*), vinblastine (*VBN*), paclitaxel (*PXL*)] were cytotoxic, evident by the increases in dead and apoptotic cells. **C,** FACS analysis of cell cycle arrest produced by SAV at 48 h. *Plots,* representative samples; *inset (gray shading),* results of data fit to cell cycle model. **D,** data from **C** with additional time points and concentrations. SAV at 10 µmol/L (*gray shading*) increased the percentage of cells in $G_1$ at both 24 and 48 h.

v1.3.8a. The mean intensities of three regions of interest were fit to a model of sequential transport, peritoneum to blood, then blood to interstitium using Graphpad Prism. Vessel intensity = $A_o \times k_1/(k_2 - k_1)(\mathrm{Exp}(-k_1 t) - \mathrm{Exp}(-k_2 t))$, where $k_1$ and $k_2$ are the rate constants for the increase (peritoneum to blood transport) and decrease (blood to interstitium transport) in vessel fluorescence, respectively. $A_o$ is a theoretical maximum fluorescence. To obtain images of the vascular and interstitial phases after SAV injection, an i.v. administration was used.

### Peak SAV Concentration in Blood

Animals (three nu/nu mice) were injected with SAV (1 mg/kg, i.p.) and blood was collected through heart puncture after anesthesia. The concentration of SAV as the dextran(Cy5) carrier in serum was determined from Cy5 fluorescence read against SAV standards in the serum of uninjected mice.

### Respiratory Burst Assay

Reactive oxygen species were measured as the luminol-dependent, horseradish peroxidase (HRP) chemiluminescence

Published OnlineFirst June 9, 2009; DOI: 10.1158/1535-7163.MCT-08-1012



in a 96-well luminometer (Centro LB 960, Berthold Technologies) in Dulbecco's PBS with calcium and magnesium (14). The HRP concentration was 20 units/mL. Where appropriate, viridin or vehicle was added with the HRP/luminol solution, 3 min before transfer to the luminometer plate.

## Results

An important difference between SAV and other viridins (7, 15, 16) was our use of fluorochromes in the SAV design. The structures of SAV and its released viridin, NBD-Wm, are shown in Fig. 1A. SAV was obtained when R is $CH_3$; however, when R is H, a control, NAV was produced. The use of fluorochromes allows the fate of SAV to be monitored *in vitro* and *in vivo* and provides useful insights into its possible mechanisms of action. The use of NBD in the SAV design was based on earlier work showing that NBD-Wm and Wm have similar activities as inhibitors of phosphoinositide-3 (PI3) kinase and cell proliferation, with NBD allowing viridin disposition to be monitored by fluorescence or by immunologic techniques (12). Cy5 was attached to the dextran so that the fate of both the pharmacologically active NBD-Wm and inert dextran(Cy5) carrier could be monitored *in vivo.* SAV and NAV differ only in the presence of a methyl group on their nitrogen atom (Fig. 1A), which dictates the ability to self-activate and the resulting bioactivity (10).

When lyophilized SAV was solubilized with PBS, release of NBD-Wm commenced. At 676 Da, NBD-Wm was far smaller than SAV (MW 72 kDa), and when released from dextran formed a precipitate identified as NBD-Wm by mass spectrometry (data not shown). A half-time of 9.2 hours for NBD-Wm generation by SAV was obtained from the changes in the absorption spectra of the supernatant lacking NBD-Wm (Fig. 1B). Cy5 absorption (maximum absorption at 650 nm) was independent of NBD-Wm release, whereas NBD-Wm absorption (maximum absorption at 480 nm) decreased due to precipitation. NBD-Wm was highly soluble in PBS when present as the prodrug SAV, due to the hydrophilic dextran carrier, but poorly soluble when released (see Fig. 1A).

The activity of NBD-Wm, SAV, and NAV as inhibitors of PI3 kinase or cell proliferation depends on the amount of the active species, NBD-Wm, present or generated over the duration of the assay. This, in turn, is dependent on the kinetics of its generation from the inactive prodrug

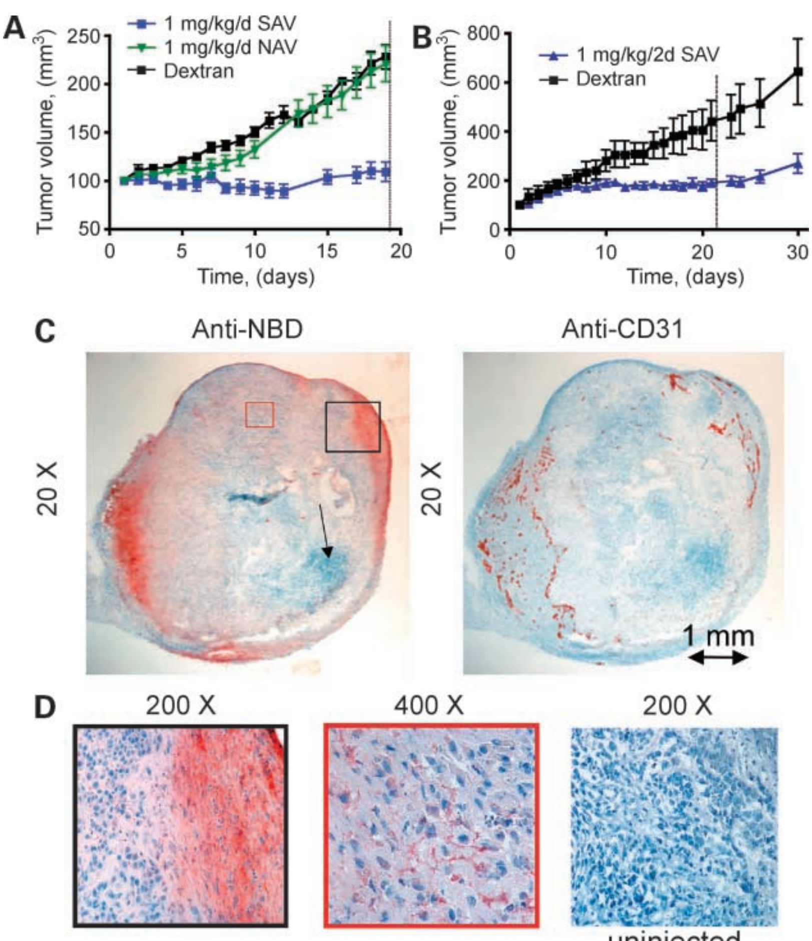


**Figure 4.** Effect of SAV on A549 tumor xenograft growth and the disposition of NBD-Wm within the tumor. **A,** antiproliferative effect of SAV and NAV at 1 mg/kg/d i.p. SAV promptly halted tumor growth whereas NAV and dextran were ineffective. **B,** antiproliferative effect of SAV at 1 mg/kg/2 d. Tumor growth stopped more slowly than in **A**. When dosing was discontinued (*dotted line*), tumor growth resumed. **C,** visualization of NBD-Wm disposition in the tumor following SAV treatment using anti-NBD immunohistochemistry. Anti-NBD or anti-CD31 staining is in red. Low magnification (20×) views of adjacent tumor sections stained with anti-NBD or anti-CD31 after a single injection of SAV (1 mg/kg, i.p.) were obtained. Anti-CD31 stain showed endothelial cells and vessels at the tumor periphery or tumor capsule. NBD-Wm was present at high concentrations in CD31-rich regions such those within the black box. NBD-Wm was also present in low concentrations in some CD31 sparse regions (*red box*) and missing from some areas devoid of CD31 (*arrow*). **D,** higher magnification views of areas defined from **B**. Views of a CD31-rich (*black box* from **C**) or central CD31-poor region (*red box* from **C**) of the anti-NBD–stained section shown in Fig. 5B. Tumor from an uninjected animal, which failed to bind anti-NBD, is also shown. Magnifications are given above each panel.

Published OnlineFirst June 9, 2009; DOI: 10.1158/1535-7163.MCT-08-1012



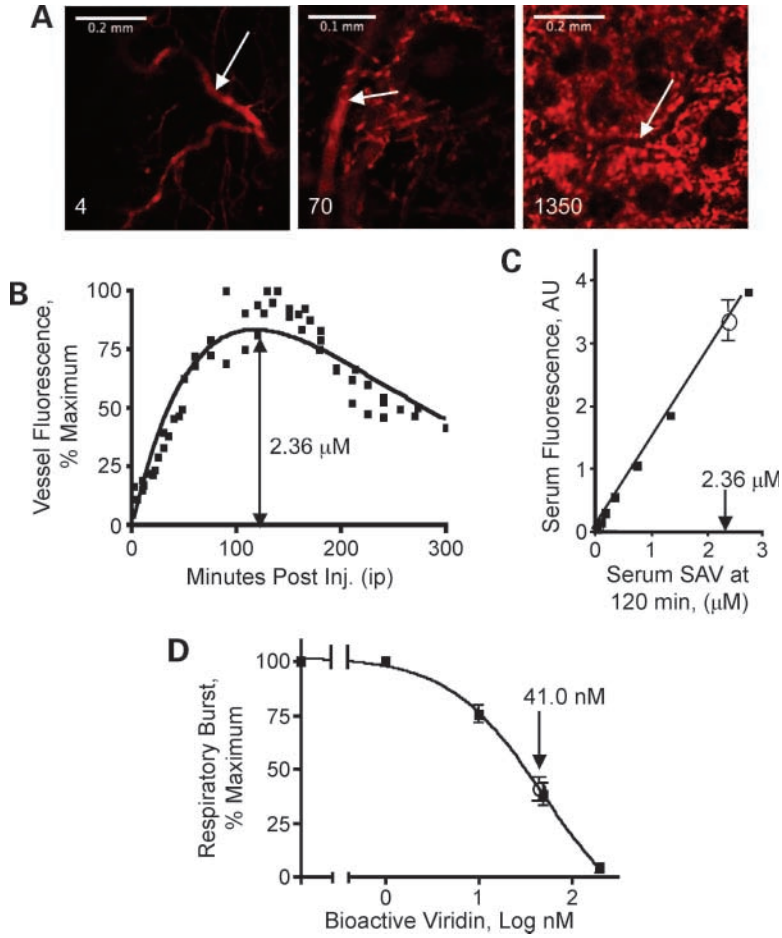


**Figure 5.** Behavior of SAV *in vivo*. **A,** intravital microscopy of SAV, seen as dextran(Cy5) fluorescence after an i.v. injection, showing vascular and interstitial phases of SAV pharmacokinetics. Vessel fluorescence of a mouse ear is shown. At 4 min postinjection, a bright vessel (*arrow*) and dark interstitial space were seen. At 1,350 min, a dark blood vessel (*arrow*) and bright interstitium were seen. At 70 min, SAV is both vascular and interstitial. **B,** time dependence of ear blood vessel fluorescence after an i.p. SAV injection with the method shown in **A**. Vessel fluorescence increased as SAV moved from the peritoneum to the blood and decreased as SAV moved from the vasculature to the interstitial space. Data were fit to a three compartment sequential transport model to obtain half-times for the transfer of SAV from the peritoneum to the blood ($t_{1/2}$ = 1.35 h) and blood to the interstitial space ($t_{1/2}$ = 1.34 h). **C,** determination of the SAV concentration in mouse serum at 120 min post i.p. injection. A standard curve (*black boxes*) of serum fluorescence versus SAV concentration was generated by adding SAV to the serum of normal, noninjected mice. Serum from SAV-injected mice was 2.36 ± 0.60 μmol/L SAV ($n$ = 3). **D,** determination of bioactive viridin levels in mice at 120 min post i.p. injection. A standard curve (*black boxes*) for the inhibition of respiratory burst was obtained using increasing concentrations of viridin and neutrophils from non–SAV-injected mice. Neutrophils from SAV-injected mice (○) had a partial inhibition of their respiratory burst equivalent to an exposure to 41.0 nmol/L viridin ($n$ = 3).

form. The half-times of viridin formation by SAV (9.2 h) or NAV (>100 h), their $IC_{50}$s as inhibitors of PI3 kinase, and their $IC_{50}$s as inhibitors of A549 cell proliferation have been reported (9). SAV had an $IC_{50}$ of 453 nmol/L as a PI3 kinase inhibitor, ~20 times higher than NBD-Wm, which had an $IC_{50}$ of 24.2 nmol/L. However, quite the opposite relation was obtained in the antiproliferative assay where the SAV $IC_{50}$ of 1.05 μmol/L was ~12 times lower than that of

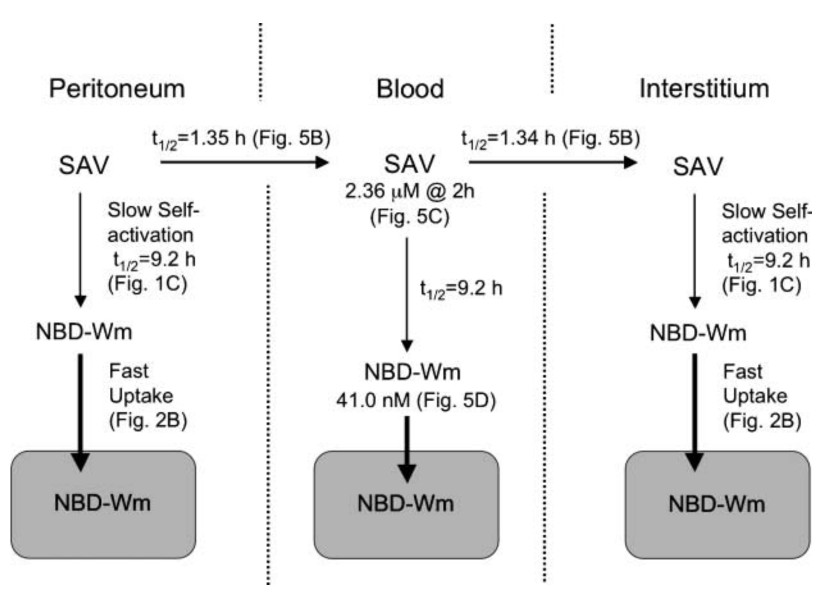


**Figure 6.** Model of SAV behavior after i.p. injection. A three-compartment model for the behavior of SAV was used to summarize the data described in previous figures. SAV self-activation had a half-time of 9.2 h (Fig. 1C). As SAV was transported from the peritoneum to blood and from the blood to the interstitium (Fig. 5B), it self-activated, releasing NBD-Wm that was rapidly internalized by cells (Fig. 2B). At 120 min post i.p. injection, the SAV concentration in blood was 2.36 μmol/L (Fig. 5C). The concentration of bioactive viridin "seen" by neutrophils was 41 nmol/L (Fig. 5D).

NBD-Wm (12.2 μmol/L). The reason for this is shown in Fig. 1C: With the 0.5-hour PI3 kinase assay, the bulk of the viridin was present as the inactive SAV prodrug (release $t_{1/2}$ = 9.2 h) and only small amounts of active NBD-Wm were released. During the 48-hour antiproliferative assay, SAV slowly released nearly all of its NBD-Wm. The necessity of NBD-Wm release from the dextran carrier for kinase inhibition is shown by results with NAV. Due to its relatively slow release (release $t_{1/2}$ >100 h), NAV failed to generate NBD-Wm over the course of the assay and thus failed to inhibit PI3 kinase.

To gain further insight into the role of NBD-Wm release in conjunction with the activity of SAV, cells were incubated with 10 μmol/L NBD either as NBD-Wm or as the self-activating SAV or nonactivating NAV, and cell fluorescence as a function of time was determined by FACS in the Fl1 channel. Figure 2A shows the fluorescence of cells incubated with each compound for 1 hour, as well as for control cells. A relative cellular fluorescence (RCF) was calculated as the mean fluorescence of treated cells (*red*, *green*, or *blue lines*) divided by that of untreated cells (*black*). At 1 hour with NBD-Wm, a RCF of 136 ± 22 was obtained, compared with a RCF of 14.1 ± 2.0 with SAV and a RCF of only 1.23 ± 0.04 with NAV, confirming rapid uptake of the small-molecule NBD-Wm by cells. With SAV, NBD-Wm slowly and progressively entered cells, reaching a peak RCF of 72.4 ± 8.7 after 24-hour incubation (Fig. 2B), consistent with slow self-activation and slow release of NBD-Wm that occurs in PBS (Fig. 1C). In contrast, cells incubated with the non-NBD-Wm–releasing NAV had a cell fluorescence of only 2.49 ± 0.13 at the 24-hour point. Cellular fluorescence from the SAV dextran(Cy5) carrier was not detectable until the incubation period reached 24 hours (data not shown) and then only reached a RCF of 2.6 ± 0.5, suggesting that NBD-Wm enters cells independently of the dextran(Cy5) carrier.

Figure 2C shows fluorescent micrographs of cells incubated for 1 hour with 10 μmol/L NBD-Wm, either as NBD-Wm or SAV. Consistent with FACS measurements (Fig. 2B), cell fluorescence by microscopy increased far more slowly with SAV than NBD-Wm. To compare intracellular NBD accumulation, the fluorescence intensity from the two images was altered to be comparable (Fig. 2C). Intracellular NBD localization was similar with SAV or NBD-Wm and was associated with perinuclear membranes, identified by the comparison of NBD fluorescence with that of membrane- and nuclear-specific stains (12). We also compared the intracellular NBD and Cy5 fluorescence after cells were incubated with SAV for 24 hours. Cy5 fluorescence was punctate in appearance and differed from intracellular membrane NBD fluorescence. Thus, both the kinetics and intracellular fluorescence localization indicated that a separation of NBD-Wm from the dextran(Cy5) carrier had occurred.

A model of SAV extracellular self-activation with the release of bioactive NBD-Wm into culture media is depicted in Fig. 2D. The model differs from the many targeting approaches that rely on a feature of the intracellular environment to separate drug from its inactive carrier (low pH, enzymes, reducing environment; ref. 11). The model is based on the following observations: (*a*) SAV slow release of NBD-Wm in PBS (9); (*b*) the slow increase in cell NBD fluorescence seen when cells were incubated with SAV, compared with rapid increase seen with NBD-Wm (Fig. 2B); (*c*) the lack of cellular uptake of NBD-Wm when attached to hydrophilic dextran through a nonreleasing linkage (NAV; Fig. 2B); and (*d*) the similar pattern of intracellular fluorescence seen with NBD-Wm and SAV (Fig. 2C), suggesting the same entity (NBD-Wm) had entered cells in both cases. As explained below, the model shown in Fig. 2D reflects the rates of uptake of SAV, NAV, and NBD-Wm (Fig. 2A), which in turn reflect their physical properties and release kinetics (see Discussion). The model proposes that SAV is a nontargeted, slow-release prodrug form of NBD-Wm.

We next assessed the cytotoxicity of SAV on A549 cells using the same conditions used for the determination of the SAV antiproliferative $IC_{50}$ of 1.05 μmol/L (single addition, 48-hour treatment). As shown with the dual-wavelength FACS analysis of Fig. 3A, 10 μmol/L SAV failed to affect the percentages of dead, apoptotic, or healthy cells. (Healthy cells = propidium iodide and Annexin V negative; apoptotic cells = Annexin V positive and propidium iodide negative; dead cells = propidium iodide positive, regardless of Annexin V binding.) Data from Fig. 3A with two additional experiments ($n$ = 3) were tabulated as shown in Fig. 3B, which indicated that SAV at 10 μmol/L had no statistically significant effect on the percentages of healthy, dead, or apoptotic cells ($P$ > 0.05). Although increasing the SAV concentration to 100 μmol/L produced modest increases in dead and apoptotic cells ($P$ < 0.05 for all), this concentration was 42 times higher than the peak serum concentration measured in our experiments and ~100 times greater than the antiproliferative $IC_{50}$. As shown in Fig. 3B, other chemotherapeutic agents produced far greater cytotoxic effects than 10 or 100 μmol/L SAV, when used at similar concentrations (10 μmol/L camptothecin) or far lower concentrations (1 μmol/L vinblastine or 0.1 μmol/L paclitaxel). Using our assay technique and A549 cells, we determined antiproliferative $IC_{50}$s of 60 nmol/L for camptothecin, 0.35 nmol/L for vinblastine, and 6.8 pmol/L for paclitaxel. From Fig. 3, we conclude that the treatment of cells with 10 μmol/L SAV was antiproliferative and without a cytotoxic effect, the latter defined as a failure to increase the proportions of dead or apoptotic cells. Treatment of cells with 100 μmol/L SAV was moderately cytotoxic, producing a small but significant increase in dead and apoptotic cells. Other chemotherapeutic agents (camptothecin, vinblastine, and paclitaxel) were highly cytotoxic, evident by the large increases in dead and apoptotic cells.

We next examined the effects of SAV on the cell cycle as shown in Fig. 3C, with data from these experiments and additional studies summarized in Fig. 3D. Treatment with 10 μmol/L SAV (results highlighted in gray in Fig. 3D) for 24 hours resulted in a marked increase in cells in $G_1$ and a slight decrease in $G_2$, results consistent with a block at $G_1$. A more modest, although still significant, escalation of $G_1$ remained in effect with cells treated for 48 hours with SAV,

Published OnlineFirst June 9, 2009; DOI: 10.1158/1535-7163.MCT-08-1012



consistent with its slow-release properties. By comparison, treatment with 10 μmol/L Wm resulted in similar significant cell cycle changes at 24 hours, but had no measurable effects at 48 hours. Treatment with 100 μmol/L SAV for 24 hours resulted in a marked decrease in cells in S and an increase in $G_2$-M. Thus, this high SAV concentration resulted in a block at $G_1$ with an additional block occurring at $G_2$. Based on Fig. 3, we conclude that a SAV concentration of 10 μmol/L (4.2 times peak serum concentration of 2.36 μmol/L and 9.5 times the antiproliferative $IC_{50}$ of 1.05 μmol/L) did not induce apoptosis or cell death, but produced a $G_1$ block in the cell cycle associated with an inhibition of cell proliferation.

The antiproliferative activity of SAV, together with the disposition of viridin in the A549 xenograft tumor model, was examined as shown in Fig. 4. At 1 mg/kg/d, i.p., SAV produced a prompt cessation of tumor growth, whereas equivalent doses of NAV or dextran were without effect. Thus, NBD-Wm release was required for the antiproliferative effects of SAV on cultured cells (9), for NBD-Wm uptake by cultured cells (Fig. 2B), and for its antiproliferative effect *in vivo*. When the dosing interval of SAV was decreased to one injection every 2 days (Fig. 4B), tumor growth was halted, but more slowly than in Fig. 4A (one injection per day). Tumor growth resumed when dosing was discontinued (*dotted line*). Animals suffered no weight loss, an effect indicative of the hyperglycemia, which can be caused by PI3 kinase inhibitors blocking insulin-mediated glucose uptake (17). Animals appeared completely normal in the duration of the treatment regimen.

The intratumoral disposition of SAV associated with its antiproliferative effects (Fig. 4A and B) was obtained by NBD immunohistochemistry on three tumors, a typical example of which is shown in Fig. 4C. Here, tumors were sectioned and the disposition of NBD and CD31 obtained on adjacent sections using anti-NBD and anti-CD31 antibodies. At low magnification (Fig. 4C), tissue NBD-Wm disposition was heterogeneous within the tumor, with high levels of NBD associated with CD31-rich regions (e.g., area shown with a black box) and lower but detectable concentrations seen in more central areas (e.g., red box). Finally, some areas of tumor were apparently free of viridin (*arrow*). Figure 4D shows NBD distribution at higher magnification from a CD31-rich area (*black box*, Fig. 4C) and central area (*red box*). NBD from central areas was found in cell membranes, whereas tumor from an uninjected animal failed to bind anti-NBD.

We next examined the behavior of SAV in mice by intravital microcopy as shown in Fig. 5. Figure 5A shows micrographs of the Cy5 fluorescence in a mouse ear obtained by intravital microscopy after an i.v. injection of SAV. At 4 minutes post injection, SAV was present in the vasculature (*white arrow*) but exhibited rapid extravasation (70 minutes). At 1,350 minutes, a purely interstitial phase was obtained, with a vessel seen as a dark tube (*white arrow*) against a fluorescent background of interstitium. Data for vessel fluorescence as a function of time after i.p. injection, the mode of administration used in xenograft (Fig. 4), were then analyzed as shown in Fig. 5B (three mice). Vessel fluorescence increased gradually, reflecting peritoneal to vascular transport, and fell due to passage of the agent from the blood to the interstitium. Using a model of sequential transport between three compartments, half-times for the transport from the peritoneum to blood and blood to interstitium of 1.35 and 1.34 hours were obtained, respectively. However, the kinetics of vessel fluorescence provided no information regarding the vascular concentrations of SAV. Therefore, we determined the serum concentration of SAV at 2-hour post-injection, the time of peak serum levels following i.p. injection (Fig. 5C). Here, the Cy5 fluorescence from SAV-injected animals was analyzed against standards prepared by adding SAV to the serum of uninjected animals. The SAV concentration in serum was determined to be 2.36 ± 0.60 μmol/L.

Having determined the time course of SAV transport between compartments and peak serum concentration, we next determined the concentration of bioactive NBD-Wm in serum using as a bioassay the degree of inhibition of the neutrophil respiratory burst from SAV-injected animals. Wm is not only an inhibitor of cell proliferation but a potent inhibitor of a number of immune functions, including neutrophil respiratory burst with reported $IC_{50}$s of 28 nmol/L (18) and 12 nmol/L (19). As shown in Fig. 5D, the respiratory burst from SAV-injected animals was compared with a standard curve obtained by adding viridin to the neutrophils obtained from non–SAV-injected mice. An $IC_{50}$ of 48.3 nmol/L was obtained for the standard curve that used neutrophils from a non–SAV-injected mouse, whereas an $IC_{50}$ of 8.6 nmol/L was obtained with human neutrophils used by others using our assay methodology.[4] The inhibition of respiratory burst from SAV-injected animals was then measured and the bioactive viridin concentration *in vivo* was calculated to be 41.0 nmol/L. We conclude that SAV exerted both an antiproliferative effect on A549 cells and inhibited the respiratory burst from neutrophils. In addition, the concentration of bioactive viridin (41.0 nmol/L) was far below serum concentrations of viridin present as the inactive prodrug, SAV (2.36 μmol/L), the implications of which are discussed below.

A pharmacokinetic model that summarizes the known features of SAV *in vitro* and *in vivo* behavior is shown in Fig. 6, which also indicates the origin of supporting data. The half-times of SAV transport from blood to the peritoneum (1.35 hours) and blood to interstitium (1.34 hours) were shorter than the half-time of self-activation and NBD-Wm generation (9.2 hours; ref. 9), indicating that substantial transport of NBD-Wm attached to dextran, that is as SAV, occurred between these three compartments. The model neglects the transport of release bioactive agent, NBD-Wm, between compartments due to its physical properties (poor solubility; Fig. 1B) and rapid internalization of NBD-Wm by cells (Fig. 2B). The peak concentration of SAV in blood (2 hours post i.p.) was 2.36 μmol/L, whereas the

[4] C. Ellson, M.B. Yaffe, and L. Josephson, unpublished observations.

Published OnlineFirst June 9, 2009; DOI: 10.1158/1535-7163.MCT-08-1012



concentration of bioactive NBD-Wm in serum was 41.0 nmol/L, based on the partial inhibition of respiratory burst activity (Fig. 5C). Thus, SAV served as a polymeric reservoir of inactive NBD-Wm, slowly self-activating to generate 41 nmol/L of the active viridin, NBD-Wm, when its serum concentration was 2.36 μmol/L.

## Discussion

The physical and pharmacokinetic properties of SAV, together with its slow self-activation, distinguish it both from other natural product–based viridin kinase inhibitors (15, 16) and from fully synthetic, man-made inhibitors (20, 21). The attachment of NBD-Wm to the 70-kDa dextran(Cy5) imbued the NBD-Wm with physical properties of dextran: a molecular weight of 72 kDa, water solubility, and membrane impermeability. Conversely, SAV self-activation released NBD-Wm and resulted in a reversal of this transformation: The released NBD-Wm was hydrophobic, of low molecular weight (676 Da), poorly soluble in water (Fig. 1B), and rapidly entered cells (Fig. 2B). Thus, the model of SAV behavior shown in Fig. 2D is consistent with our data and the general principles governing the physical properties of membrane-permeable materials.

Regarding the pharmacokinetic properties of SAV, Kaneo has shown that the blood half-time of a 70 kDa dextran in mice was 1.59 hours, in good agreement with our value for the SAV blood half-time of 1.34 hours (22). We also found that SAV underwent transport from the vascular compartment to the interstitium (Fig. 5A), consistent with studies on the pharmacokinetics of fluorescent dextrans in mice (23). We therefore conclude that the physical and pharmacokinetic properties of SAV were determined by its 70-kDa dextran carrier.

We initially showed that SAV slowly released its viridin in PBS (Fig. 1B) and then in cell culture (Fig. 2B). To show the role SAV self-activation and viridin release played *in vivo*, we showed that NAV, identical to SAV except for a methyl group needed for self-activation (Fig. 1A), failed to inhibit tumor growth (Fig. 4A). Not only was NBD-Wm release crucial for the antiproliferative effect of SAV on the A549 tumor but our observations also indicate that *in vivo* SAV served as a reservoir of inactive prodrug generating low levels of NBD-Wm (Fig. 5C and D). Based on the partial inhibition of neutrophil respiratory burst, the apparent concentration of bioactive viridin was 41.0 nmol/L, whereas the serum level of NBD-Wm present as the inactive prodrug was 2.36 μmol/L. SAV therefore circulates as an inactive prodrug in micromolar concentration range, self-activating to generate nanomolar concentrations of active viridin.

To determine whether the antiproliferative effects of SAV *in vivo* were due to its effects on A549 cells, its effects on those cells in culture were examined. SAV (10 μmol/L) blocked the proliferation of A549 cells (antiproliferative $IC_{50}$ = 1.05 μmol/L; ref. 9) but did not induce cell death or apoptosis. In contrast, the antiproliferative effects of three standard chemotherapeutic agents (paclitaxel, camptothecin, and vinblastine) were associated with increases in apoptosis (Annexin V binding) and cell death (propidium iodide binding). SAV (10 μmol/L) increased the proportion of cells in the $G_1$ phase of the cell cycle at both 24 and 48 hours, whereas effects of Wm were qualitatively similar but transient, with cells returning to control behavior at 48 hours. A similar short-duration effect of Wm on the cell cycle has been observed (24).

Although SAV had clear effects on A549 cells, it seems that the cytostatic effects of SAV on the tumor were not due solely to its effects on tumor cells. First, the intratumoral distribution of NBD-Wm after SAV injection showed that NBD-Wm concentrated in the vascularized tumor periphery or capsule (Fig. 4C), with lower concentrations in the central portion of the tumor and some areas free of NBD-Wm altogether. Second, the antiproliferative $IC_{50}$ of SAV was 1.05 μmol/L, a considerable improvement in potency from the $IC_{50}$ of 12.2 μmol/L obtained with NBD-Wm (9). However, the peak serum concentration of SAV seen at 2 hours post i.p. injection was only 2.36 μmol/L, a level that will not produce the complete inhibition of growth of the A549 tumor obtained based on the *in vitro* antiproliferative $IC_{50}$ (1.05 μmol/L). Of note is the fact that a single peak of SAV of 2.36 μmol/L once per 48 hours was sufficient to inhibit tumor growth (a dosing of SAV at 1 mg/kg/2 d was sufficient to inhibit tumor growth, see Fig. 4B). Third, Wm is a potent inhibitor of angiogenesis but a rather weak inhibitor of tumor cell proliferation. Wm and NBD-Wm have similar, weak antiproliferative activities, with $IC_{50}$s using the A549 cell line of 11.4 and 12.2 μmol/L, respectively (9). Similar $IC_{50}$s have been obtained with NBD-Wm and Wm for other tumor cell lines (12). In contrast, Wm is a potent inhibitor of angiogenesis, with an $IC_{50}$ in the nanomolar range with the chick embryo chorioallantoic membrane model (25).

The use of frequent low doses of chemotherapeutic agents, with the goal of inhibiting tumor angiogenesis, can be an alternative to successive rounds of high-dose chemotherapy where the goal is tumor eradication (1). Two SAV properties, its cytostatic activity and its ability to slowly generate low concentrations of active viridin, suggest that SAV could be used as a metronomic chemotherapeutic agent. Future studies with SAV might be directed to examining it as a component of long-term, multidrug, metronomic therapeutic approaches.

## Disclosure of Potential Conflicts of Interest

No potential conflicts of interest were disclosed.

### References

1. Kerbel RS, Kamen BA. The anti-angiogenic basis of metronomic chemotherapy. Nat Rev Cancer 2004;4:423–36.

2. Wipf P, Halter Robert J. Chemistry and biology of wortmannin. Org Biomol Chem 2005;3:2053–61.

3. Hanson JR. The viridin family of steroidal antibiotics. Nat Prod Rep 1995;12:381–4.

4. Wymann MP, Bulgarelli-Leva G, Zvelebil MJ, et al. Wortmannin inactivates phosphoinositide 3-kinase by covalent modification of Lys-802, a residue involved in the phosphate transfer reaction. Mol Cell Biol 1996; 16:1722–33.

5. Yuan H, Barnes KR, Weissleder R, Cantley L, Josephson L. Covalent

Published OnlineFirst June 9, 2009; DOI: 10.1158/1535-7163.MCT-08-1012



reactions of wortmannin under physiological conditions. Chem Biol 2007;14:321–8.

**6.** Norman BH, Shih C, Toth JE, et al. Studies on the mechanism of phosphatidylinositol 3-kinase inhibition by wortmannin and related analogs. J Med Chem 1996;39:1106–11.

**7.** Creemer LC, Kirst HA, Vlahos CJ, Schultz RM. Synthesis and *in vitro* evaluation of new wortmannin esters: potent inhibitors of phosphatidylinositol 3-kinase. J Med Chem 1996;39:5021–4.

**8.** Schultz RM, Merriman RL, Andis SL, et al. *In vitro* and *in vivo* antitumor activity of the phosphatidylinositol-3-kinase inhibitor, wortmannin. Anticancer Res 1995;15:1135–9.

**9.** Blois J, Yuan H, Smith A, et al. Slow self-activation enhances the potency of viridin prodrugs. J Med Chem 2008;51:4699–707.

**10.** Yuan H, Luo J, Weissleder R, Cantley L, Josephson L. Wortmannin-C20 conjugates generate wortmannin. J Med Chem 2006;49:740–7.

**11.** Kratz F, Muller IA, Ryppa C, Warnecke A. Prodrug strategies in anticancer chemotherapy. ChemMedChem 2008;3:20–53.

**12.** Barnes KR, Blois J, Smith A, et al. Fate of a bioactive fluorescent wortmannin derivative in cells. Bioconjug Chem 2008;19:130–7.

**13.** Darzynkiewicz Z, Juan G, Bedner E. Current protocols in cell biology. New York: John Wiley & Sons; 1999.

**14.** Ellson CD, Davidson K, Ferguson GJ, O'Connor R, Stephens LR, Hawkins PT. Neutrophils from p40phox−/− mice exhibit severe defects in NADPH oxidase regulation and oxidant-dependent bacterial killing. J Exp Med 2006;203:1927–37.

**15.** Zask A, Kaplan J, Toral-Barza L, et al. Synthesis and structure-activity relationships of ring-opened 17-hydroxywortmannins: potent phosphoinositide 3-kinase inhibitors with improved properties and anticancer efficacy. J Med Chem 2008;51:1319–23.

**16.** Ihle NT, Williams R, Chow S, et al. Molecular pharmacology and antitumor activity of PX-866, a novel inhibitor of phosphoinositide-3-kinase signaling. Mol Cancer Ther 2004;3:763–72.

**17.** Powis G, Ihle N, Kirkpatrick DL. Practicalities of drugging the phosphatidylinositol-3-kinase/Akt cell survival signaling pathway. Clin Cancer Res 2006;12:2964–6.

**18.** Baggiolini M, Dewald B, Schnyder J, Ruch W, Cooper PH, Payne TG. Inhibition of the phagocytosis-induced respiratory burst by the fungal metabolite wortmannin and some analogues. Exp Cell Res 1987;169:408–18.

**19.** Arcaro A, Wymann MP. Wortmannin is a potent phosphatidylinositol 3-kinase inhibitor: the role of phosphatidylinositol 3,4,5-triphosphate in neutrophil responses. Biochem J 1993;296:297–301.

**20.** Knight ZA, Gonzalez B, Feldman ME, et al. A pharmacological map of the PI3-K family defines a role for p110α in insulin signaling. Cell 2006;125:733–47.

**21.** Ruckle T, Schwarz MK, Rommel C. PI3Kγ inhibition: towards an 'aspirin of the 21st century'? Nat Rev Drug Discov 2006;5:903–18.

**22.** Kaneo Y, Uemura T, Tanaka T, Kanoh S. Polysaccharides as drug carriers: biodisposition of fluorescein-labeled dextrans in mice. Biol Pharm Bull 1997;20:181–7.

**23.** Dreher MR, Liu W, Michelich CR, Dewhirst MW, Yuan F, Chilkoti A. Tumor vascular permeability, accumulation, and penetration of macromolecular drug carriers. J Natl Cancer Inst 2006;98:335–44.

**24.** Rosenzweig KE, Youmell MB, Palayoor ST, Price BD. Radiosensitization of human tumor cells by the phosphatidylinositol 3-kinase inhibitors wortmannin and LY294002 correlates with inhibition of DNA-dependent protein kinase and prolonged $G_2$-M delay. Clin Cancer Res 1997;3:1149–56.

**25.** Oikawa T, Shimamura M. Potent inhibition of angiogenesis by wortmannin, a fungal metabolite. Eur J Pharmacol 1996;318:93–6.

Published OnlineFirst June 9, 2009; DOI: 10.1158/1535-7163.MCT-08-1012



Molecular Cancer Therapeutics

# The antiproliferative cytostatic effects of a self-activating viridin prodrug

Adam Smith, Joseph Blois, Hushan Yuan, et al.

*Mol Cancer Ther* 2009;8:1666-1675. Published OnlineFirst June 9, 2009.